

# SUBMILLIMETER QUASI-PERIODIC OSCILLATIONS IN MAGNETICALLY CHOKED ACCRETION FLOWS MODELS OF SGR A\*

ROMAN V. SHCHERBAKOV<sup>1,2,3</sup>, JONATHAN C. MCKINNEY<sup>2,4</sup>

*Draft version May 1, 2013*

## ABSTRACT

High-frequency quasi-periodic oscillations (QPOs) appear in general-relativistic magnetohydrodynamic simulations of magnetically choked accretion flows around rapidly rotating black holes (BHs). We perform polarized radiative transfer calculations with our ASTRORAY code in order to explore the manifestations of these QPOs for Sgr A\*. We construct a simulation-based model of a radiatively inefficient accretion flow and find model parameters by fitting the mean observed polarized source spectrum. The simulated QPOs have a total sub-mm flux amplitude of under 5% and a linearly polarized flux amplitude of up to 2%. The oscillation period  $T \approx 100M \approx 35$  min corresponds to the rotation period of the BH magnetosphere that produces a trailing spiral in resolved disk images. The total flux signal is statistically significant over noise for all tested frequencies 87 GHz, 230 GHz, and 857 GHz and inclination angles  $10^\circ$ ,  $37^\circ$ , and  $80^\circ$ . The non-detection in the 230 GHz Sub-Millimeter Array light curve is consistent with a low signal level and low sampling rate. The possible presence of such magnetospheric QPOs in Sgr A\* will be better tested with Atacama Large Millimeter Array.

*Subject headings:* accretion, accretion disks — black hole physics — Galaxy: center — instabilities — magnetohydrodynamics (MHD) — radiative transfer

## 1. INTRODUCTION

Quasi-periodic oscillations (QPOs) in the emission from black hole (BH) accretion disks and jets are found in systems with both stellar mass BHs (Remillard & McClintock 2006) and supermassive BHs (SMBHs) (Gierliński et al. 2008; Reis et al. 2012). High-frequency QPOs (HFQPOs) with period  $T$  that is similar to the orbital period at the innermost stable circular orbit (ISCO) potentially probe the region close to the BH event horizon, offering a chance to test accretion and jet theories in the strong gravity regime. There have been multiple claims of HFQPOs from the SMBH Sgr A\* in the Milky Way center, which then provides a unique opportunity to study HFQPOs up-close. Henceforth, we set the speed of light and gravitational constant to unity ( $c = 1$  and  $G = 1$ ), such that  $1M = 21$  s for Sgr A\* with BH mass  $M_{\text{BH}} = 4.3 \times 10^6 M_{\odot}$  (Ghez et al. 2008; Gillessen et al. 2009).

A HFQPO period commonly claimed to be seen in Sgr A\* is  $T = 17\text{min} = 48M$ . This was identified in the K band during a flare (Genzel et al. 2003), in 7 mm data by Yusef-Zadeh et al. (2011), and in images obtained with very long baseline interferometry (VLBI) by Miyoshi et al. (2011). Periods of  $T = 28\text{min} = 79M$  (Genzel et al. 2003),  $T = 23\text{min} = 65M$ , and  $T = 45\text{min} = 127M$  (Trippe et al. 2007; Hamaus et al. 2009) were reported in IR observations of flares. However, Do et al. (2009) analyzed a long K band light curve and did not find power spectrum density excess to be statistically significant at any period. A statistically significant longer period of  $T = 2.5 - 3\text{hrs} \approx 470M$  was reported by Mauerhan et al. (2005) in 3 mm data. Miyoshi et al. (2011) found a range of periods from 17 min to 56 min claiming to

see the spirals with multiple arms, but did not perform significance analysis.

The physical origins of HFQPOs are highly debated. Models are often based on the ISCO orbital frequency, the epicyclic frequency, and the frequencies of various pressure and gravity modes (see Kato 2001, 2004; Remillard & McClintock 2006; Wagoner 2008 for an overview). Some underlying physical origins may be beat frequencies (van der Klis 2000), resonances between flow modes and normal frequencies in general relativity (GR) (Abramowicz & Klužniak 2001), trapped oscillations (Nowak & Wagoner 1991), parametric resonance (Abramowicz et al. 2003), and disk magnetospheric oscillations (Li & Narayan 2004).

Such analytic methods have been followed by searches for QPOs in magnetohydrodynamic (MHD) simulations. Non-GR 2D MHD simulations by Tagger & Melia (2006); Falanga et al. (2007) exhibited spiral patterns of Rossby waves detectable in simulated light curves. Non-GR 3D MHD simulations of thick accretion disks by Chan et al. (2009) developed QPOs with a period  $T = 39M$ <sup>5</sup> in simulated X-ray light curve. A similar search in thin disk simulations (Reynolds & Miller 2009) yielded no QPOs. The 3D GRMHD simulations and radiative transfer by Schnittman et al. (2006) revealed weak transient QPOs. Similar simulations by Dolence et al. (2012) post-processed with radiative transfer code *grmonty* (Dolence et al. 2009) showed a spiral structure producing oscillations with periods  $T = 6 - 9\text{min} = 17 - 25M$  in simulated NIR and X-ray light curves. GRMHD simulations of tilted disks produce low quality oscillations in dynamical quantities with  $T \approx 170M = 1$  hr (Henisey et al. 2012).

Such MHD simulations start with a weak magnetic field, which is amplified by the magneto-rotational instability (MRI) that generates incoherent turbulence. However, when magnetized gas falls onto a BH, the disk can become sat-

roman@astro.umd.edu

<sup>1</sup><http://astroman.org>

Department of Astronomy, University of Maryland, College Park, MD 20742, USA

<sup>2</sup>Joint Space Science Institute, University of Maryland, College Park MD 20742, USA

<sup>3</sup>Hubble Fellow

<sup>4</sup>Physics Department, University of Maryland, College Park, MD 20742-4111, USA

<sup>5</sup>We rescale reported periods to the current value of Sgr A\* BH mass.

urated with more magnetic flux than the MRI can generate (McKinney et al. 2012). 3D GRMHD simulations of radiatively inefficient accretion flows (RIAFs, as applicable to SgrA\*) with ordered magnetic flux were performed by McKinney et al. (2012). The resultant magnetically chocked accretion flow (MCAF) has a BH magnetosphere that significantly affects the sub-Keplerian equatorial inflow. The simulations showed high-quality disk-BH magnetospheric QPOs in dynamical quantities with an  $m = 1$  (one-arm) toroidal mode and a rotating inflow pattern in the equatorial plane. Such magnetospheric QPOs are robust to significant tilt between the disk and BH spin (McKinney et al. 2013).

In present paper, we quantify the QPO signal and its statistical significance in simulated Sgr A\* light curves for flow models based on GRMHD simulations of MCAFs. In Section 2 we describe the 3D GRMHD simulations and the application to Sgr A\*. We perform GR polarized radiative transfer calculations with our ASTRORAY code and fit Sgr A\* mean polarized spectrum. We find the best-fitting accretion rate  $\dot{M}$ , electron temperature  $T_e$ , and the BH spin inclination angle  $\theta$ , which is coincident with the viewing angle. In Section 3 we describe timing analysis. We study the light curves of the best-fitting model viewed at different  $\theta$ . We find QPOs to be statistically significant in total and linearly polarized (LP) fluxes. While the largest absolute flux variations are achieved in total flux, the largest relative variations are exhibited in LP flux. We image a correspondent equatorial plane spiral wave. In Section 4 we compare the simulated QPO amplitudes and periods with those of observed Sgr A\* oscillations. We argue that the non-detection in 230 GHz Submillimeter Array (SMA) data is consistent with the low level of simulated QPOs, but future Atacama Large Millimeter Array (ALMA) observations may detect sub-mm Sgr A\* oscillations.

## 2. SGR A\* MODEL BASED ON GRMHD SIMULATIONS

### 2.1. GRMHD Simulations

The initial gas reservoir is a hydrostatic torus (Gammie et al. 2003) within which magnetic field loops are inserted. The MRI action on the initial field leads to MHD turbulent accretion that eventually causes magnetic flux to saturate near the BH (McKinney et al. 2012). We focus on a simulation with a dimensionless spin  $a_* = 0.9375$ , which is similar to  $a_* \approx 0.9$  favored in simulation-based modeling of Sgr A\* spectrum and the emitting region size (Mościbrodzka et al. 2009; Dexter et al. 2010; Shcherbakov et al. 2012). The simulation is performed in spherical coordinates  $(r, \theta, \phi)$  with resolution  $N_r \times N_\theta \times N_\phi = 272 \times 128 \times 256$ . It reached a quasi-steady state by time  $t = 8,000M$  and ran till  $t = 28,000M$ . In steady state near the BH event horizon, the sub-Keplerian inflow is balanced against the BH magnetosphere resulting in vertical compression of the disk.

The BH magnetosphere and disk exhibit QPOs in dynamical quantities such as the magnetic field energy density. A toroidal wobbling mode with  $m = 1$  is eminent in the jet polar region and disk plane. They were identified with pattern rotation of the BH magnetospheric region pierced by the infalling matter streams. The streams form due to magnetic Rayleigh-Taylor instabilities (e.g. Stone & Gardiner 2007). The pattern rotates with an angular frequency  $\Omega_F \approx 0.2\Omega_H$ , where  $\Omega_H = a_*/(2r_H)$  is the BH angular frequency and  $r_H = (1 + \sqrt{1 - a_*^2})M$  is the horizon radius. The angular frequency  $\Omega_F$  is similar to the rotation frequency  $\approx 0.27\Omega_H$  of the field

lines attached to the BH at the equatorial plane in paraboloidal magnetospheric solution (Blandford & Znajek 1977).

### 2.2. Sgr A\* Accretion Flow Model

We use this 3D GRMHD simulation of an MCAF to model the Sgr A\* accretion flow. We follow Shcherbakov et al. (2012) to define the electron temperature and continuation of quantities to radii  $r$  outside of  $50M$ . A power-law extension of density to  $r > 50M$  is  $n \propto r^{-\beta}$ , while the proton temperature is continued as  $T_p \propto r^{-1}$ . The magnetic field is extended as  $b \propto \sqrt{nT_p} \propto r^{(-1-\beta)/2}$  to preserve a constant ratio of the magnetic field energy density to the thermal energy density. The slope  $\beta$  is found by connecting the known density at  $r = 3 \times 10^5 M$  to the density in the inner region (Shcherbakov & Baganoff 2010). Correct simultaneous evolution of the simulations and the radiation field is considered, despite radiative transfer is conducted in post-processing.

We focus on the accretion disk as the source of emission from Sgr A\* and will consider jet emission (e.g., Falcke et al. 2004) in future studies. The simulation's matter densities are artificial near the polar axis because matter is injected in order to avoid an exceedingly high local ratio of magnetic energy to rest-mass energy that is difficult for GRMHD codes to evolve. The injected material does not change flow dynamics because it's locally energetically negligible. However, a small amount of hot matter in the polar region can shine brightly as revealed by Mościbrodzka et al. (2009). The matter densities are zeroed out in a bipolar cone with an opening angle  $\theta = 26^\circ$ . If that artificial matter was not removed, then none of our models would be consistent with the observed image size at 230 GHz (Doeleman et al. 2008) and the observed polarized Sgr A\* spectrum.

Radiative transfer is performed with our ASTRORAY code (Shcherbakov & Huang 2011; Shcherbakov et al. 2012). We compute radiation over a quasi-steady simulation period between  $t = 8,000M$  and  $t = 28,000M$ . Following our previous work, we fit the total flux of Sgr A\* at 87–857 GHz, the LP fraction at 87 GHz, 230 GHz, and 345 GHz, and the circular polarization (CP) fraction at 230 GHz and 345 GHz. We vary the heating constant  $C$ , which determines the electron temperature  $T_e$  close to the BH, the accretion rate  $\dot{M}$ , and the inclination angle  $\theta$ . Comparing the mean Sgr A\* spectrum with the mean simulated spectra we reach  $\chi^2/\text{dof} = 1.55$  for  $\text{dof} = 9$ , which is a better fit than our prior work based on weakly magnetized simulations (Penna et al. 2010; Shcherbakov et al. 2012). The correspondent values of parameters are  $T_e = 3.2 \times 10^{10} \text{ K}$  at  $6M$  distance from the center,  $\dot{M} = 1.0 \times 10^{-8} M_\odot \text{ yr}^{-1}$ , and  $\theta = 37^\circ$ . We then perform timing analysis of the model, which reproduces Sgr A\* spectrum.

## 3. TIMING ANALYSIS

### 3.1. Oscillations in Light Curves and Images

Let us first demonstrate oscillations in the light curves. In Figure 1 we show the light curves between times  $t = 25,500M$  and  $t = 26,100M$  for the best-fitting model with the inclination angle  $\theta = 37^\circ$ . The light curves are shown at three frequencies with different optical depth: radiation at 87 GHz is optically thick, the optical depth at 230 GHz is about  $\tau \sim 1$ , while radiation is optically thin at 857 GHz. The total flux (top panel) shows regular oscillations with the amplitude  $\Delta F \approx 0.05 \text{ Jy}$  at 87 GHz and  $\Delta F \approx 0.15 \text{ Jy}$  at 230 GHz. Fluctuations at 857 GHz with the amplitude  $\Delta F \approx 0.2 \text{ Jy}$  are less regular.

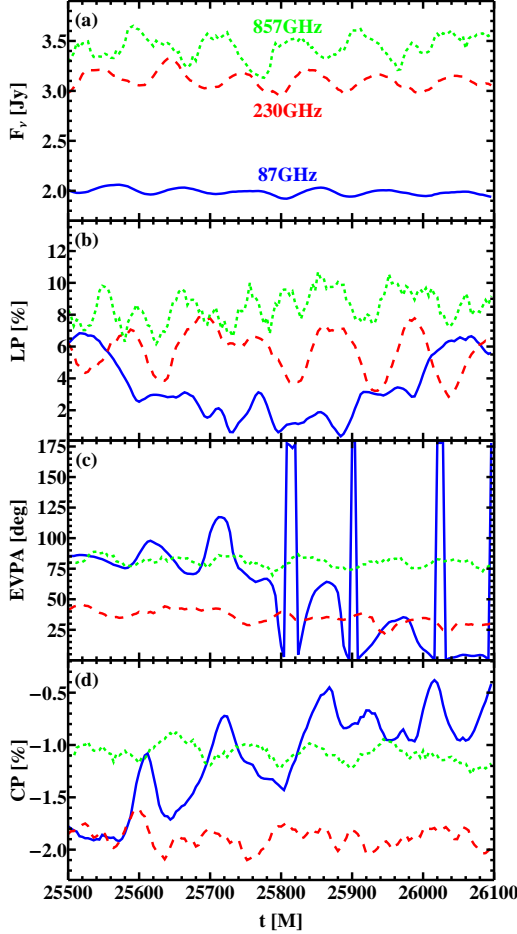


FIG. 1.— Fragments of the light curves for the best-fitting model with the inclination angle  $\theta = 37^\circ$  at optically thick 87 GHz (blue solid line), at 230 GHz (red dashed line) with the optical depth about unity, and at optically thin 857 GHz (green dotted line).

The LP fraction fluctuates at 2% level at all three frequencies, which translates into relative variations of up to 50% and absolute LP flux variations of  $\Delta F \approx 0.06$  Jy. The LP and CP fractions and the electric vector position angle (EVPA) exhibit substantial variations over long timescales at 87 GHz. Variations of the EVPA at 230 GHz and 857 GHz are about  $5^\circ - 10^\circ$ . The CP fraction oscillates by 0.3% at 87 GHz and by 0.15% at higher frequencies. Absolute CP flux variations are  $\Delta F \approx 0.005$  Jy at 230 GHz.

In Figure 2 we show how the amplitude of oscillations depends on the inclination angle  $\theta$  at 230 GHz. Shown are the light curves for the best-fitting inclination angle  $\theta = 37^\circ$  (solid line), for almost face-on  $\theta = 10^\circ$  (dashed line), and for almost edge-on  $\theta = 80^\circ$  (dotted line). The total flux shows the same amplitude  $\Delta F \approx 0.15$  Jy regardless of  $\theta$ . The edge-on and the best-fitting cases produce comparable variations of the LP fraction, while cancellations of the polarized fluxes emitted in different regions lower both the mean and the fluctuation amplitude of the LP fraction in the face-on case. Correspondingly, the EVPA fluctuates dramatically in the face-on case. The CP fraction oscillates at 0.5% level in the edge-on case, while the other cases exhibit 0.15% amplitude of CP oscillations.

The face-on accretion flow images with  $\theta = 10^\circ$  are shown

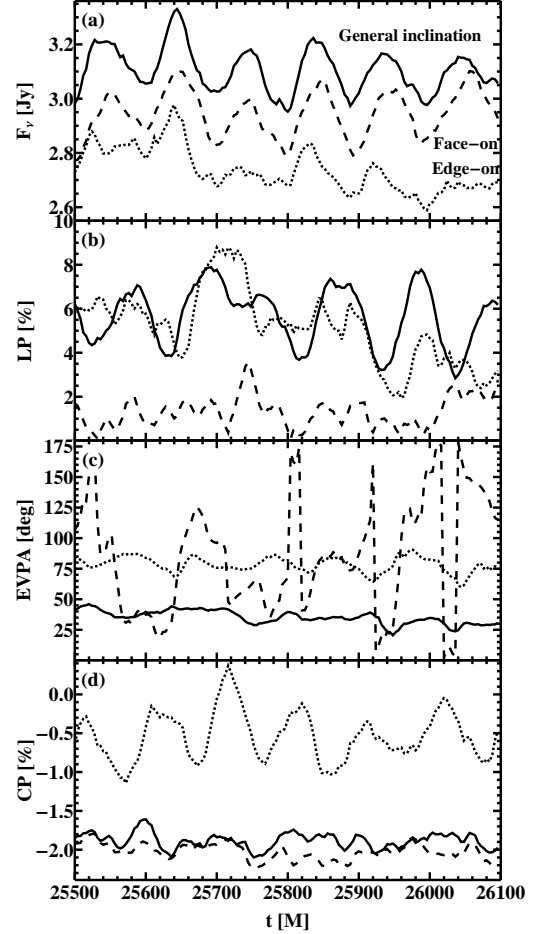


FIG. 2.— Fragments of the light curves at 230 GHz for the best-fitting  $T_e$  and  $\dot{M}$  and several inclination angles  $\theta$ : best-fitting  $\theta = 37^\circ$  (solid), face-on  $\theta = 10^\circ$  (dashed), and edge-on  $\theta = 80^\circ$  (dotted).

in Figure 3. We put the time series of the total intensity images in the top row and the time series of the LP intensity images in the bottom row. The total intensity images show a clear one-arm spiral, which rotates with a period of  $T \approx 100M \approx 35$  min. A spiral of LP intensity is offset from the spiral of total intensity, as the region of the brightest total intensity exhibits the strongest LP cancellations. Our total intensity spiral looks similar to that in Dolence et al. (2012), despite different angular velocities. Note that we report the intensity images, while Dolence et al. (2012) showed the images of the dynamical quantities.

### 3.2. Statistical Analysis

Let us quantify the significance of QPOs. Following Papadakis & Lawrence (1993) we start with an autocovariance

$$\hat{R}(k) = \frac{1}{N} \sum_{t=1}^{N\Delta t - |k|} (x_t - \bar{x})(x_{t+|k|} - \bar{x}), \quad (1)$$

where  $k = 0, \pm 1\Delta t, \dots, \pm(N-1)\Delta t$  and  $x_t$  is the sample of simulated fluxes normalized to have its mean  $\bar{x}$  equal unity. We then compute a periodogram

$$I(R) = \frac{\Delta t}{2\pi} \sum_{k=-(N-1)\Delta t}^{(N-1)\Delta t} \hat{R}(k) \cos \omega k, \quad -\frac{\pi}{\Delta t} \leq \omega \leq \frac{\pi}{\Delta t}. \quad (2)$$

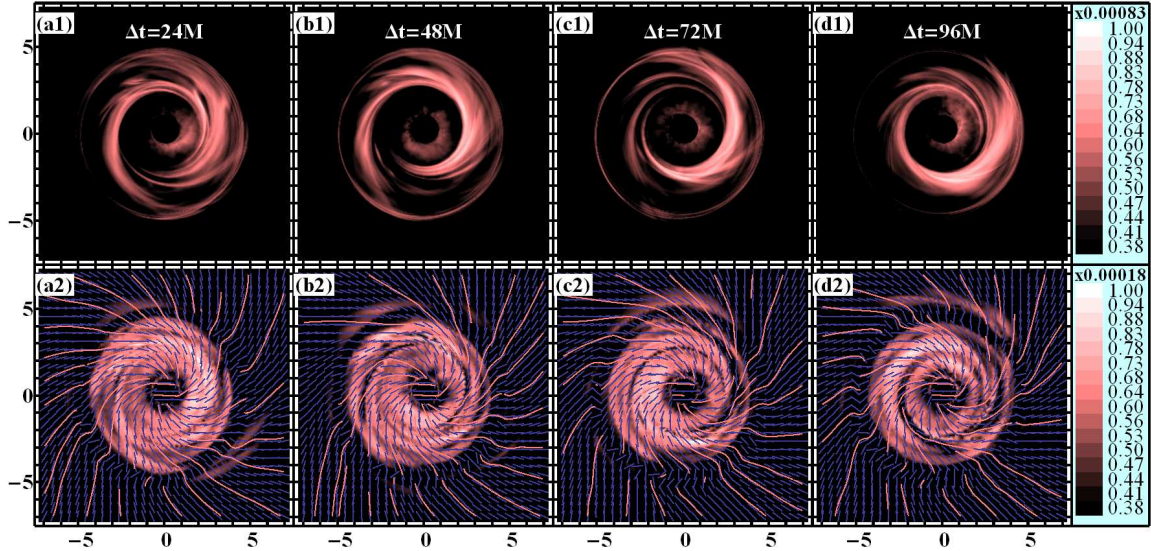


FIG. 3.— Images of a face-on disk at 230 GHz: total intensity images (top row) and LP intensity images (bottom row). Strokes indicate the EVPA direction. The rotating spiral pattern is clearly visible.

In our analysis  $\Delta t = 4M$ , which appears large enough to avoid aliasing at periods  $T > 50M$ . All periodograms are log-smoothed to 0.08dex following Papadakis & Lawrence (1993).

Determination of the statistical significance of QPOs involves comparison of the simulated periodogram with random noise periodograms. We follow the procedure in Timmer & Koenig (1995) to generate random noise. We employ a log-smoothed to 3.0dex periodogram of the simulated light curve to normalize the noise power, which eliminates power spectrum peaks and introduces less bias compared to fitting the simulated periodogram with a powerlaw. We draw the Fourier transform of random noise from a normalized Gaussian distribution and perform the inverse Fourier transform to generate the light curve. We then compute random noise autocovariance and periodogram. We find a  $3\sigma$  significance curve based on 2,592 random noise samples.

Periodograms with correspondent  $3\sigma$  significance curves are depicted in Figure 4 for a number of frequencies and inclination angles. The top curves in each panel are for almost face-on inclination  $\theta = 10^\circ$ , the middle curves are for  $\theta = 37^\circ$ , and the bottom curves are for almost edge-on  $\theta = 80^\circ$ . QPOs with a given period are statistically significant, if a periodogram rises above the  $3\sigma$  curve at that period. The total flux and the LP fraction periodograms exhibit statistically significant peaks with the period  $T \approx 100M$  at most studied frequencies and inclination angles. However, a face-on disk generally shows weaker QPOs, which are not significant at 857 GHz. LP fraction oscillations are weak for a face-on disk at all frequencies due to random cancelations of the LP. The total flux and the LP fraction at 230 GHz show the strongest signal indicating that current active efforts to observe at 1.3 mm wavelength are the most promising for QPOs. Oscillations with a period  $T = 1000M \approx 4$  hr are detected with  $3\sigma$  significance in LP fraction. We characterize presence of oscillations and stability of an oscillation period by a spectrogram in Figure 5. The spectrogram indicates that most of the time oscillations with a period  $T = 90 - 100M$  are present. However, no oscillations occur around time  $t = 22,000M$ , when a burst of accretion is caused by weaker magnetic field.

#### 4. DISCUSSION AND CONCLUSIONS

##### 4.1. Summary and Comparison to Previous Work

In this paper we report QPOs in simulated Sgr A\* light curves for a model based on the state-of-the-art 3D GRMHD simulations of magnetically chocked RIAFs. By adjusting the parameters we find a fit with  $\chi^2/\text{dof} = 1.55$  for dof = 9 to the mean sub-mm source spectrum. Correspondent simulated total flux light curve shows regular oscillations with the period  $T \approx 100M \approx 35$  min and the amplitude  $\Delta F \approx 0.15$  Jy at 230 GHz. Less regular fluctuations with  $\Delta F \approx 0.2$  Jy are seen at 857 GHz. Weaker oscillations with  $\Delta F \approx 0.05$  Jy are seen at 87 GHz, which probes the optically thick emission from  $\sim 10M$  radius. The LP fraction exhibits periodic modulations at 50% relative level, but the absolute LP flux amplitude is only about  $\Delta F \approx 0.06$  Jy. QPOs are significant at a  $3\sigma$  level in the total flux light curves for all tested inclination angles  $10^\circ$ ,  $37^\circ$ , and  $80^\circ$  and frequencies 87 GHz, 230 GHz, and 857 GHz, while the LP fraction shows less prominent QPOs at 87 GHz and in a face-on case.

Our main  $T \approx 35$  min period is longer than the claimed observed 17–20 min period of Sgr A\*, while the simulated periods  $T = 6 - 9$  min in Dolence et al. (2012) are shorter. Their simulation has the same BH spin  $a_* = 0.9375$  as in our simulation, but Dolence et al. (2012) simulations evolve to below saturation levels for the magnetic flux near the BH and to a somewhat thin disk with height-to-radius ratio of  $H/R \sim 0.2$ . The resultant MRI-dominated accretion flow has Keplerian rotation and shorter QPO periods. They did not identify their QPO mechanism, although they noted their turbulence is unresolved (Shiokawa et al. 2012) and this might lead to artificial QPOs (Henisey et al. 2009). Our MCAF model has sub-Keplerian rotation and QPOs driven by the rotating BH magnetosphere’s actions on the disk (Li & Narayan 2004) that leads to longer periods. Our relatively thick disk with  $H/R \sim 0.6$  is similar to expected for a RIAF, and our simulations well-resolve disk turbulence (McKinney et al. 2012) suggesting the QPOs are robust. Based upon these works, Sgr A\* QPOs might be explained by  $a_* = 0.9375$  with an intermediate gas rotation rate, magnetization, or  $H/R$ .

Flow cooling, whose marginal importance for Sgr A\* was

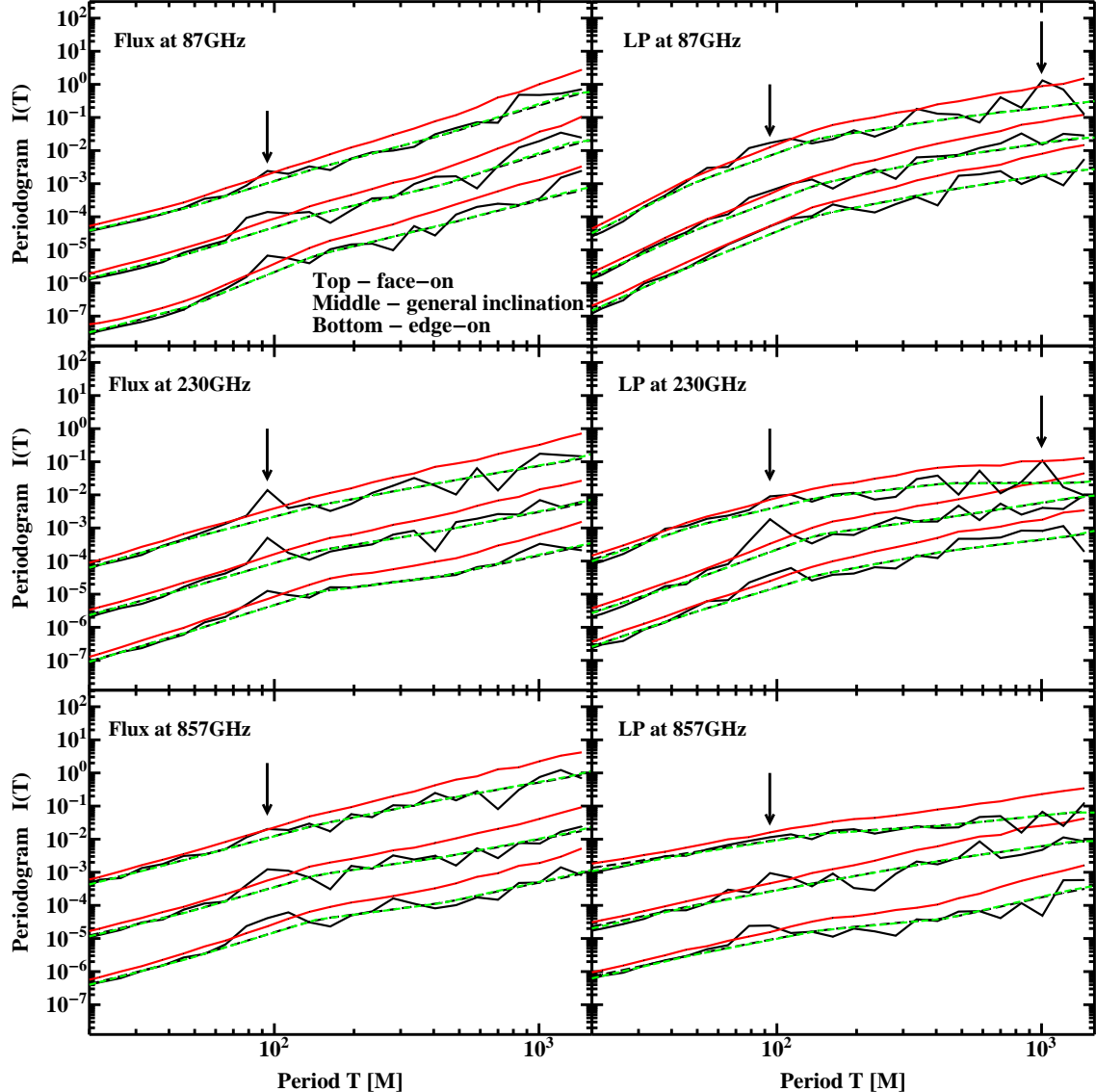


FIG. 4.— Periodograms of the total flux and the LP fraction light curves for the frequencies 87 GHz, 230 GHz, and 857 GHz and the inclination angles  $\theta = 10^\circ$  (top curves in each panel),  $\theta = 37^\circ$  (middle curves), and  $\theta = 80^\circ$  (bottom curves), while  $T_c$  and  $\dot{M}$  are fixed at their best-fitting values: simulated periodograms (dark black solid lines),  $3\sigma$  significance curves (light red solid lines), log-smoothed to 3.0dex simulated periodograms (dark black dashed lines), and geometric means of random noise periodograms (light green dashed lines).

suggested by Drappeau et al. (2012), can self-consistently choose the disk thickness  $H/R$  in simulations. In MCAFMs, the steady-state BH horizon magnetic flux has a positive correlation with  $H/R$  (McKinney et al. 2012), so cooling can lead to less sub-Keplerian rotation rates and a weaker magnetosphere, and then the the QPO period from MCAFMs could be comparable to claimed for Sgr A\*.

#### 4.2. Observing QPOs in Sgr A\*

We showed that QPOs, though significant, have maximum amplitude of 5% or  $\Delta F \sim 0.15$  Jy in the sub-mm. Low sensitivity and low sampling rate of current sub-mm instruments might prohibit observational detection of such oscillations (Marrone 2006). SMA achieves an accuracy of 5% and sampling every 10 min at 1.3 mm with a correspondent 20 min Nyquist period (Marrone et al. 2008). Thus, a weak signal with  $T \sim 30$  min period can be readily masked by aliasing and noise in SMA data. Caltech Submillimeter

Observatory (CSO) is comparable with SMA in sensitivity and sampling rate (Marrone et al. 2008). Very Large Array (VLA) provides exceptional signal-to-noise ratio and sampling rate to detect QPOs at higher wavelengths. Indeed, Yusef-Zadeh et al. (2011) find QPOs in Sgr A\* VLA light curve at 43 GHz with the amplitude  $\Delta F \sim 0.03$  Jy, which is similar to our predicted  $\Delta F \sim 0.05$  Jy at 87 GHz. Yet, oscillations are prominent on only 1 of 5 nights in VLA data, which may indicate intermittency of QPOs in the Galactic Center. Our modeling provides a potential reason for such intermittency: QPOs are practically absent when the magnetic field is weak due destruction by magnetic field reversals.

The total flux QPO amplitude  $\Delta F \approx 0.15$  Jy is larger than the LP flux amplitude  $\Delta F \approx 0.06$  Jy. However, the observational error of the total flux can also be larger. SMA can measure the LP flux up to the leakage level of  $\sim 0.3\%$ , while the total flux is only measured to  $\sim 1\%$  due to calibration uncertainties (Marrone et al. 2007). Then it is about equally dif-

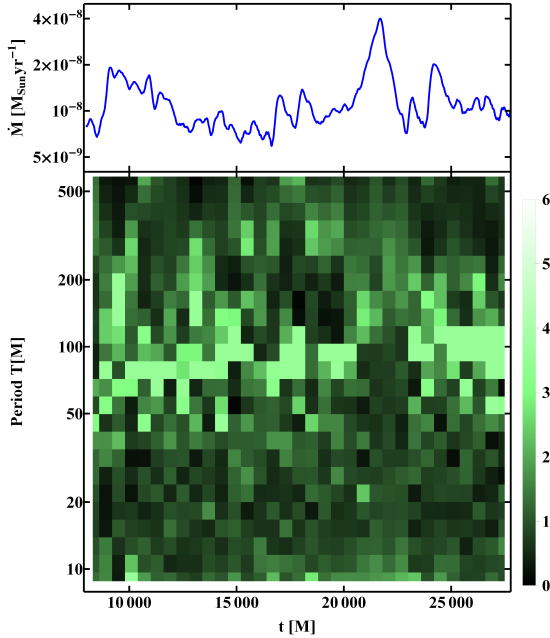


FIG. 5.— Accretion rate dependence on time  $\dot{M}(t)$  (top) and normalized spectrogram of the total flux light curve (bottom) for simulation intervals with  $\Delta t = 600M$ . The normalized spectrogram is made up of ratios of log-smoothed to 0.08dex periodograms over log-smoothed to 3.0dex periodograms. The higher ratio and the lighter color indicate QPOs.

ficult to detect total flux oscillations and LP flux oscillations. ALMA gives more hope than older observatories in detecting Sgr A\* sub-mm QPOs. ALMA covers a wide range of sub-mm frequencies 84 – 720 GHz and has a collecting area of  $\sim 7 \times 10^3 \text{ m}^2$  (Brown et al. 2004) about 30 times the collecting area of SMA. ALMA observations of Sgr A\* are expected to have a flux error under 0.05 Jy and sampling every few minutes, which should be enough to reveal the predicted oscillations were they present on an observation night.

## 5. ACKNOWLEDGEMENTS

The authors thank Chris Reynolds and Jim Moran for comments. This work was supported by NASA Hubble Fellowship grant HST-HF-51298.01 (RVS) and NSF/XSEDE resources provided by NICS (Kraken/Nautilus) under the awards TG-AST080025N (JCM) and PHY120005 (RVS/JCM).

## REFERENCES

- Abramowicz, M. A., Karas, V., Kluźniak, W., Lee, W. H., & Rebusco, P. 2003, PASJ, 55, 467  
 Abramowicz, M. A., & Kluźniak, W. 2001, A&A, 374, L19  
 Blandford, R. D., & Znajek, R. L. 1977, MNRAS, 179, 433  
 Brown, R. L., Wild, W., & Cunningham, C. 2004, Advances in Space Research, 34, 555  
 Chan, C.-k., Liu, S., Fryer, C. L., Psaltis, D., Özel, F., Rockefeller, G., & Melia, F. 2009, ApJ, 701, 521  
 Dexter, J., Agol, E., Fragile, P. C., & McKinney, J. C. 2010, ApJ, 717, 1092  
 Do, T., Ghez, A. M., Morris, M. R., Yelda, S., Meyer, L., Lu, J. R., Hornstein, S. D., & Matthews, K. 2009, ApJ, 691, 1021  
 Doeleman, S. S., et al. 2008, Nature, 455, 78  
 Dolence, J. C., Gammie, C. F., Mościbrodzka, M., & Leung, P. K. 2009, ApJS, 184, 387  
 Dolence, J. C., Gammie, C. F., Shiokawa, H., & Noble, S. C. 2012, ApJ, 746, L10  
 Drappeau, S., Dibi, S., Dexter, J., Markoff, S., & Fragile, P. C. 2012, ArXiv e-prints  
 Falanga, M., Melia, F., Tagger, M., Goldwurm, A., & Bélanger, G. 2007, ApJ, 662, L15  
 Falcke, H., Körding, E., & Markoff, S. 2004, A&A, 414, 895  
 Gammie, C. F., McKinney, J. C., & Tóth, G. 2003, ApJ, 589, 444  
 Genzel, R., Schödel, R., Ott, T., Eckart, A., Alexander, T., Lacombe, F., Rouan, D., & Aschenbach, B. 2003, Nature, 425, 934  
 Ghez, A. M., et al. 2008, ApJ, 689, 1044  
 Gierliński, M., Middleton, M., Ward, M., & Done, C. 2008, Nature, 455, 369  
 Gillessen, S., Eisenhauer, F., Trippe, S., Alexander, T., Genzel, R., Martins, F., & Ott, T. 2009, ApJ, 692, 1075  
 Hamau, N., Paumard, T., Müller, T., Gillessen, S., Eisenhauer, F., Trippe, S., & Genzel, R. 2009, ApJ, 692, 902  
 Henisey, K. B., Blaes, O. M., & Fragile, P. C. 2012, ApJ, 761, 18  
 Henisey, K. B., Blaes, O. M., Fragile, P. C., & Ferreira, B. T. 2009, ApJ, 706, 705  
 Kato, S. 2001, PASJ, 53, 1  
 Kato, Y. 2004, PASJ, 56, 931  
 Li, L.-X., & Narayan, R. 2004, ApJ, 601, 414  
 Marrone, D. P. 2006, PhD thesis, Harvard University  
 Marrone, D. P., Moran, J. M., Zhao, J.-H., & Rao, R. 2007, ApJ, 654, L57  
 Marrone, D. P., et al. 2008, ApJ, 682, 373  
 Mauerhan, J. C., Morris, M., Walter, F., & Baganoff, F. K. 2005, ApJ, 623, L25  
 McKinney, J. C., Tchekhovskoy, A., & Blandford, R. D. 2012, MNRAS, 423, 3083  
 —. 2013, Science, 339, 49  
 Miyoshi, M., Shen, Z.-Q., Oyama, T., Takahashi, R., & Kato, Y. 2011, PASJ, 63, 1093  
 Mościbrodzka, M., Gammie, C. F., Dolence, J. C., Shiokawa, H., & Leung, P. K. 2009, ApJ, 706, 497  
 Nowak, M. A., & Wagoner, R. V. 1991, ApJ, 378, 656  
 Papadakis, I. E., & Lawrence, A. 1993, MNRAS, 261, 612  
 Penna, R. F., McKinney, J. C., Narayan, R., Tchekhovskoy, A., Shafee, R., & McClintock, J. E. 2010, MNRAS, 408, 752  
 Reis, R. C., Miller, J. M., Reynolds, M. T., Gültekin, K., Maitra, D., King, A. L., & Strohmayer, T. E. 2012, Science, 337, 949  
 Remillard, R. A., & McClintock, J. E. 2006, Ann. Rev. Astron. Astr., 44, 49  
 Reynolds, C. S., & Miller, M. C. 2009, ApJ, 692, 869  
 Schnittman, J. D., Krolik, J. H., & Hawley, J. F. 2006, ApJ, 651, 1031  
 Shcherbakov, R. V., & Baganoff, F. K. 2010, ApJ, 716, 504  
 Shcherbakov, R. V., & Huang, L. 2011, MNRAS, 410, 1052  
 Shcherbakov, R. V., Penna, R. F., & McKinney, J. C. 2012, ApJ, 755, 133  
 Shiokawa, H., Dolence, J. C., Gammie, C. F., & Noble, S. C. 2012, ApJ, 744, 187  
 Stone, J. M., & Gardiner, T. 2007, ApJ, 671, 1726  
 Tagger, M., & Melia, F. 2006, ApJ, 636, L33  
 Timmer, J., & Koenig, M. 1995, A&A, 300, 707  
 Trippe, S., Paumard, T., Ott, T., Gillessen, S., Eisenhauer, F., Martins, F., & Genzel, R. 2007, MNRAS, 375, 764  
 van der Klis, M. 2000, ARA&A, 38, 717  
 Wagoner, R. V. 2008, New Astronomy Reviews, 51, 828  
 Yusef-Zadeh, F., Wardle, M., Miller-Jones, J. C. A., Roberts, D. A., Grossi, N., & Porquet, D. 2011, ApJ, 729, 44